3D FUSION OF CINE AND LATE-ENHANCED CARDIAC MAGNETIC RESONANCE IMAGES

L. Cordero-Grande[1], *S. Merino-Caviedes*[1], *X. Albà*[2,3], *R.M. Figueras i Ventura*[2,3], *A.F. Frangi*[2,4], *C. Alberola-López*[1*]

[1] LPI, University of Valladolid (UVA), Valladolid, Spain
[2] CISTIB, DTIC, Universitat Pompeu Fabra (UPF) and CIBER-BBN, Barcelona, Spain
[3] ICREA, Barcelona, Spain
[4] Department of Mechanical Engineering, The University of Sheffield, Sheffield, UK

ABSTRACT

A procedure to fuse the information of short-axis cine and late enhanced magnetic resonance images is presented. First a coherent 3D reconstruction of the images is obtained by object-based interpolation of the information of contiguous slices in stacked short-axis cine acquisitions and by the correction of slice misalignments with the aid of a set of reference long-axis slices. Then, late enhanced stacked images are also interpolated and aligned with the anatomical information. Thus, the complementary information provided by both modalities is combined in a common frame of reference and in a nearly isotropic grid, which is not possible with existing fusion procedures. Numerical improvement is established by comparing the distances between unaligned and aligned manual segmentations of the myocardium in both modalities. Finally, a set of snapshots illustrate the improvement in the information overlap and the ability to reconstruct the gradient in the long-axis.

Index Terms— image fusion, magnetic resonance imaging, image registration, interpolation, myocardial infarction.

1. INTRODUCTION

Cardiac magnetic resonance (MR) imaging is a flexible non-invasive modality to assess the anatomy and the global and local function of the left ventricle. Moreover, with the injection of a contrast agent it is able to provide information about myocardial perfusion and scar [1]. Nevertheless, MR acquisitions are performed over a long period of time so the patient usually moves in the scanner and corresponding spatial locations, as given by the measurement machinery, do not correspond to the same material locations inside the patient body. This lack of correspondence could be worsened by the different amount of air reserve in the lungs for different acquisitions or by the inability to maintain the apnea if the patient has a serious cardiorespiratory disorder. Moreover, imaging orientations and resolutions also vary for different acquisitions so, in the whole, the correspondence of different measurement procedures is difficult to establish. Some works have emphasized this limitation as well as hypothesized about the potential benefits in overcoming it [2, 3, 4, 5].

Our approach builds a high resolution nearly isotropic joint representation of two common modalities in cardiac acquisition protocols, namely cine-MR and late enhanced (LE) MR images. Once this is accomplished, cine-derived information can be used to provide a precise representation of the myocardial boundaries whereas LE information can be used to characterize the scar extension. Not so many references have tried to spatially combine the information provided by these two modalities, [4] being probably the most outstanding[1]. In this work the authors map the information of LE and first-pass perfusion images to a common reference frame as obtained by a whole heart volume dataset. For that purpose, they tackle three subproblems: (1) the spatial alignment of slices belonging to a given image series, (2) the temporal alignment of perfusion sequences and (3) the spatial alignment to a common reference dataset. Our work focuses on the third of these points, though it also pays attention to the first one. The work in [4] gives a simplified solution for the spatial alignment of LE images to a common reference dataset in which they do not include the possible respiration-induced translation in the long-axis (LA) in their model. They claim that this is necessary in order "to preserve the volumetric information which would be changed by the interpolations resulting from a slice position change". Our work proposes a methodology to overcome this limitation by first building a coherent 3D high-resolution representation of the acquired slice stacks and then performing their alignment directly in

*This work was partially supported by the MICIIN and the FEDER under Research Grant TEC2010-17982, and by the CDTI under the cvREMOD project and Research Grant CEN-20091044. The work was also funded by the Junta de Castilla y León under Grants VA039A10-2 and VA376A11-2 and the Consejería de Sanidad de Castilla y León under Grants GRS 292/A/08, SAN126/VA032/09 and SAN126/VA033/09.

[1] Another approach is presented in [3], but it relies on a manual segmentation of the myocardium for the alignment.

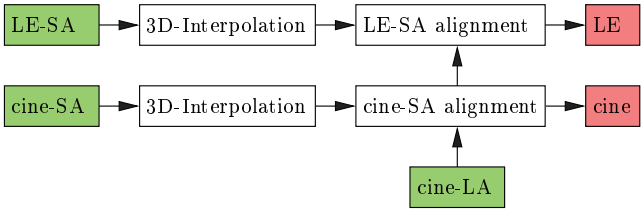


Fig. 1. Flow diagram of the algorithm.

the 3D space. To our understanding these ideas can also be applied to the first of the subproblems highlighted in [4], thus they also constitute a contribution to approaches such as [6].

An overview of the algorithm is presented in Section 2. The 3D interpolation and misalignment correction are further developed in Sections 3 and 4 respectively. Quantitative and visual validation is performed in Section 5 and some conclusions are established in Section 6.

2. OVERVIEW OF THE ALGORITHM

The algorithm flow is illustrated in Fig. 1. First, a high resolution representation of the original short-axis (SA) stacked slices acquisition is constructed as explained in Section 3. The procedure is the same for both modalities. Once a 3D representation is obtained by this procedure, the algorithm sequentially corrects for misalignment artifacts first for the cine volume by using the LA information as a reference and then for the LE volume by using the cine corrected volume as a reference. The procedure of alignment, similar for both modalities, is explained in Section 4. Hence, the result of the algorithm is a mutually aligned high-resolution nearly isotropic volumetric representation of the original datasets.

3. RECONSTRUCTION OF 3D INFORMATION

In our previous work [7], we proposed a registration method for object-based interpolation. This method is applied here in order to reconstruct the absent spatial information between the slices. Formally, denote by $I^{\text{cine}}[\mathbf{m}, n]$ the cine-MR image from which $\mathbf{m} = [m_0, m_1, m_2]$ indexes a spatial location, with m_0 referring to the rows of the SA slices, m_1 to their columns and m_2 to a SA slice, and n referring to a temporal phase. The first image in the sequence is extracted, so $n = 0$, which corresponds to end diastole[2]. We assume a coordinate system oriented in the plane of acquisition of the images and that the image resolution is given by $(\Delta_0, \Delta_1, \Delta_2)$ with $\Delta_0 = \Delta_1$, as usual. The set of slices is in the range $0 \leq m_2 \leq M_2 - 1$, with M_2 the number of slices. Then, the procedure matches each pair of slices $\{m_2^0, m_2^0 + 1\}$ and, based on the matching result, it reconstructs a set of $L - 1$ intermediate slices such that $L = [\Delta_2/\Delta_0]$, with $[\cdot]$ the operator that extracts the greatest integer value less than or equal to its argument. Then, a nearly isotropic 3D reconstruction of the original image is obtained. An analogous procedure is applied to the LE-MR image $I^{\text{LE}}[\mathbf{m}]$.

[2]The extraction of this image is based on the fact that LE-MR images are acquired approximately at the end diastolic phase.

4. CORRECTION OF MISALIGNMENT

The correction of breath-derived misalignment supposes that each original slice in the stacked acquisitions may have been subjected to a rigid transform with respect to the position derived from the scanner coordinate system. Then, if $\boldsymbol{\psi}(\mathbf{x}) = (\psi_0(\mathbf{x}), \psi_1(\mathbf{x}), \psi_2(\mathbf{x}))$ is the transform from physical to continuous pixel coordinates, the transform of a point $\mathbf{x}$ due to breath-derived misalignment can be modeled as in (1):

$$\mathbf{A}(\mathbf{x}) = (\psi_2(\mathbf{x}) - m_2)\mathbf{A}^{m_2+1}(\mathbf{x}) + (1 + m_2 - \psi_2(\mathbf{x}))\mathbf{A}^{m_2}(\mathbf{x}), \quad (1)$$

where $\mathbf{A}^{m_2}$ represents the set of rigid transforms associated with the stack of slices and $m_2 = [\psi_2(\mathbf{x})]$.

In order to simplify the transform optimization, we assume that the slice rotation is null, so the rigid transforms are indeed translations. This simplification has been used customarily [8, 9], and is based on the fact that the rotating part of the transform is usually small, so we write:

$$\mathbf{A}^{m_2}(\mathbf{x}) = \mathbf{T}^{m_2}(\mathbf{x}) = \mathbf{x} + \mathbf{t}^{m_2}, \quad (2)$$

with $\mathbf{t}^{m_2} = (t_0^{m_2}, t_1^{m_2}, t_2^{m_2})$, which is restricted by $|t_2^{m_2}| < t_2^{\max}$ in order to avoid singularities in the transformed images.

The cine-MR images are registered against a set of LA slices. In our experiments three LA slices were acquired in different orientations. From them, a volumetric image is reconstructed with the same dimensions of the high-resolution cine-MR image. For that purpose, the pixels that are outside the region captured by the LA images (as given by their orientation and slice thickness) are not considered for the metric evaluation, and when more than one LA image is present in a given pixel, their intensities are averaged. The restriction of the transform is given by $t_2^{\max} = 0$ in order to prevent for distortions in the SA corrected image due to slice spacing changes. The metric used for registration is the normalized correlation as the images contain the same information content. A gradient-descent optimization scheme is used where the step size is diminished each time the direction of the gradient changes abruptly. The parameters of the optimizer are set empirically. Linear interpolation is used to obtain the intensity of the deformed cine-MR images on a rectilinear grid.

Afterwards, the LE-MR image is aligned against the high-resolution corrected cine-MR image by establishing $t_2^{\max} = \Delta_2/3$ in order to prevent from degenerate transforms. A simple metric for multimodal registration (thus considering the different intensity content of cine-MR and LE-MR images) has been recently proposed in [10] based on the local entropy of the images, which is a measure of their local structure.

First, the local entropy is extracted from the intensities in a neighborhood of the pixel of interest $\mathcal{N}[\mathbf{m}]$ as:

$$H(\mathbf{I}[\mathcal{N}[\mathbf{m}]]) = -\frac{1}{|\mathcal{N}|}\sum_{\mathbf{n}\in\mathcal{N}[\mathbf{m}]} p(I[\mathbf{n}])\log(p(I[\mathbf{n}])). \quad (3)$$

Then, the sum of the squared differences of this feature is used as the registration metric. In our application, the number of bins for the entropy computation is set to 5 and $\mathcal{N}[\mathbf{m}] = \{\mathbf{n} : |n_i - m_i| \leq 3\ \forall i\}$, with i denoting the pixel components. The optimizer parameters are the same as in the cine-MR registration case. Linear interpolation is also used to reconstruct the deformed LE-MR images on a rectilinear grid.

5. RESULTS

In this Section we validate the fusion procedure. For that purpose, we show the improvement obtained by the alignment as given by the distance between the manual segmentation of the myocardium in cine-MR and LE-MR images both for the unaligned and aligned cases. Additionally, we offer some visual snapshots which show the ability of the method to reconstruct a coherent LA representation of the images and to align them.

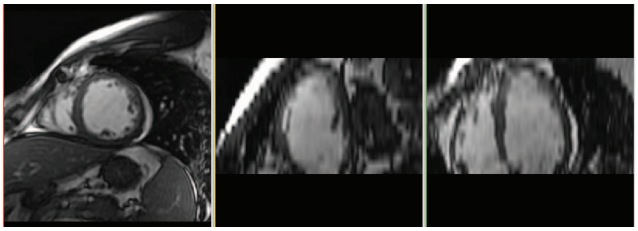
5.1. Quantitative results

To justify the validity of our fusion procedure, an expert has segmented the contours of the myocardium in each slice and modality. Then a 3D reconstruction of the myocardial surface is obtained by using the method presented in Section 3 on the distance transform of the contours. Finally, the segmented surfaces are transformed with the transform resulting from the alignment procedure. Original and transformed segmentations are then compared using both the mean and the Hausdorff surface distances[3] to evaluate the fusion performance. Improvement obtained by using the 3D interpolation scheme is also established.

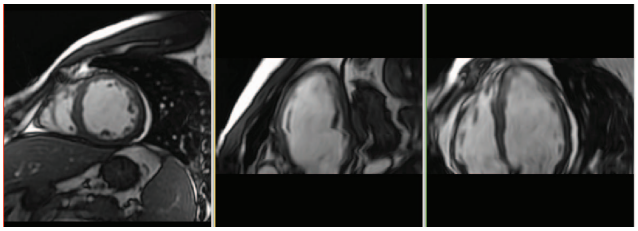
The sequences have been acquired by a GE Genesis Signa 1.5 T equipment. 4 subjects have been considered. Respective echo times for the cine-MR and LE-MR sequences are of 1.3960 ms and 4.0150 ms, repetition times are of 3.4240 ms and 9.0360 ms, inversion time of the LE-MR sequence is of 240 ms and flip angles are of 45 ° and 20 °. Pixel spacings are $\Delta_0^{\text{cine}} = 0.8594$ mm and $\Delta_0^{\text{LE}} = 0.9375$ mm with respective slice thicknesses of 6 mm and 10 mm and spacings between slices $\Delta_2^{\text{cine}} = 8$ mm and $\Delta_2^{\text{LE}} = 10$ mm.

The results are summarized in Table 1. The main conclusion is that the mean distance between the segmented surfaces is decreased by using a conventional alignment procedure and that the interpolation stage is able to further reduce this distance. Additionally, the interpolation greatly robustifies the alignment results as given by the Hausdorff distance between the surfaces. Worse results in the Hausdorff distance for the alignment without interpolation with respect to no alignment imply that in some slices this methodology is unable to obtain the actual deformation between the images, which is likely to be due to the absence of a coherent representation of the image gradient in the LA direction.

[3]These distances are computed using the Danielsson method [11].



(a) Intensity-based interpolation.



(b) Registration-based interpolation.

Fig. 2. Comparative snapshot of the interpolation procedure.

5.2. Visual results

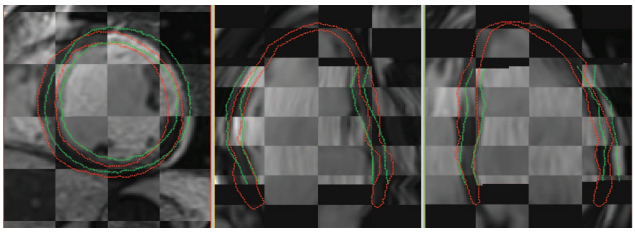
In Fig. 2, we show the results of registration-based interpolation versus linear intensity-based interpolation for the images of a cine volume. We have reconstructed three orthogonal cuts from the available information. The improvement in the definition of the gradient along the LA is clearly appraised in the interpolated images, which avoid the so-called staircase effect. In Fig. 3, we show a checkerboard representation of the aligned versus the non-aligned (but interpolated) images, where cine-MR and LE-MR myocardial segmentations are plotted in red and green respectively. The misalignment of the non-aligned case is greatly diminished in the aligned case (see for instance the endocardium in the SA images).

6. CONCLUSIONS AND FUTURE WORK

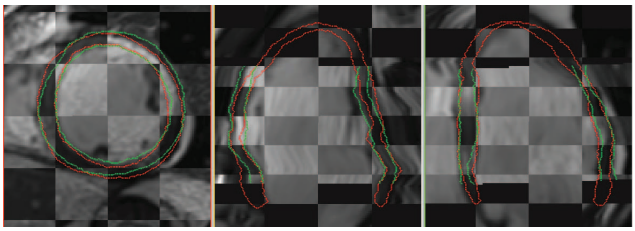
We have presented a method for the spatial fusion of cine and LE MR cardiac images which is based on the reconstruction of their 3D information and the correction of breath-derived motion artifacts. Though applied to the aforementioned modalities due to the particular interest of their fusion in clinical practice (the myocardium segmentation, being a necessary preprocessing step to obtain the scar extension, is difficult in LE images), the method is generic, so it can be applied to the fusion of other MR cardiac imaging protocols. In particular we plan to adapt this method for the fusion of cine

Table 1. Averaged surface errors (in mm) for different alignment procedures.

Alignment	Mean			Hausdorff		
	Endocardium	Epicardium	Myocardium	Endocardium	Epicardium	Myocardium
None	2.269	2.272	1.739	9.422	8.681	9.439
Without interpolation	1.974	2.054	1.536	10.749	10.079	10.985
With interpolation	1.563	1.495	1.272	7.759	6.942	7.793



(a) Interpolated images.



(b) Aligned images.

Fig. 3. Comparative snapshot of the alignment procedure.

SA and LA stacked acquisitions [6], where we expect that the interpolation step will also improve the registration accuracy. Additionally, we plan to fuse perfusion images as in [4] in order to jointly analyze common contrast-enhanced acquisition protocols. Finally, the proposed fusion pipeline could help to perform a joint 3D segmentation of the images and enables to construct 3D representations of the infarcted tissue.

7. ACKNOWLEDGMENT

The authors would like to thank the ICICOR of the Hospital Clínico de Valladolid (Spain) for providing the images and manual segmentations used in this work.

8. REFERENCES

[1] A.K. Attili, A. Schuster, E. Nagel, J.H.C. Reiber, and R.J. van der Geest, "Quantification in cardiac MRI: advances in image acquisition and processing," *Int. J. Cardiovasc. Imaging*, vol. 26, pp. 27–40, 2010.

[2] T. Mäkelä, P. Clarysse, O. Sipilä, N. Pauna, Q.C. Pham, T. Katila, and I.E. Magnin, "A review of cardiac image registration methods," *IEEE Trans. Med. Imaging*, vol. 21, no. 9, pp. 1011–1021, Sept. 2002.

[3] C. Swingen, R.T. Seethamraju, and M. Jerosch-Herold, "An approach to the three-dimensional display of left ventricular function and viability using MRI," *Int. J. Cardiovasc. Imaging*, vol. 19, pp. 325–336, 2003.

[4] A. Hennemuth, A. Seeger, O. Friman, S. Miller, B. Klumpp, S. Oeltze, and H.-O. Peitgen, "A comprehensive approach to the analysis of contrast enhanced cardiac MR images," *IEEE Trans. Med. Imaging*, vol. 27, no. 11, pp. 1592–1610, Nov. 2008.

[5] A.A. Young and A.F. Frangi, "Computational cardiac atlases: from patient to population and back," *Exp. Physiol.*, vol. 94, no. 5, pp. 578–596, 2009.

[6] A. Elen, J. Hermans, J. Ganame, D. Loeckx, J. Bogaert, F. Maes, and P. Suetens, "Automatic 3-D breath-hold related motion correction of dynamic multislice MRI," *IEEE Trans. Med. Imaging*, vol. 29, no. 3, pp. 868–878, Mar. 2010.

[7] L. Cordero-Grande, G. Vegas-Sánchez-Ferrero, P. Casaseca de-la Higuera, and C. Alberola-López, "A Markov random field approach for topology-preserving registration: application to object-based tomographic image interpolation," *IEEE Trans. Image Process.*, 2011, in press.

[8] J. Lötjönen, M. Pollari, S. Kivistö, and K. Lauerma, "Correction of movement artifacts from 4-D cardiac short- and long-axis MR data," in *MICCAI. Lect. Notes Comput. Science*. Springer-Verlag Berlin Heidelberg, 2004, vol. 3217, pp. 405–412.

[9] J. Barajas, K.L. Caballero, J. Garcia Barnés, F. Carreras, S. Pujadas, and P. Radeva, "Correction of misalignment artifacts among 2-D cardiac MR images in 3-D space," in *MICCAI Workshop Comput. Vis. Intravascular Intracardiac Imag.*, 2006, pp. 114–121.

[10] C. Wachinger and N. Navab, "Entropy and Laplacian images: Structural representations for multi-modal registration," *Med. Image Anal.*, vol. 16, no. 1, pp. 1–17, 2012.

[11] P.-E. Danielsson, "Euclidean distance mapping," *Comput. Graph. Image Process.*, vol. 14, pp. 227–248, 1980.